BEAM INDUCED FLUORESCENCE PROFILE MONITOR DEVELOPMENTS

P. Forck*, C. Andre, F. Becker, R. Haseitl, and B. Walasek-Höhne
GSI Helmholtzzentrum für Schwerionenforschung, Darmstadt, Germany

Abstract

As conventional intercepting diagnostics will not withstand high intensity ion beams, the non-destructive Beam Induced Fluorescence (BIF) method for transverse profile monitoring was extensively developed during the last years at the GSI heavy ion facility. Tests with various ions in the energy range from 1.4 MeV/u to 750 MeV/u were done. An overview of the general performance and the technical realization is given. Fluorescence spectra of nitrogen and rare gases were recorded, using an imaging spectrograph and wavelength selected beam profiles were obtained. The recorded transverse profiles coincides for all working gases with the exception of *He*. The background contribution by beam induced neutrons and γs was investigated.

BIF METHOD OVERVIEW

Non-destructive transverse profile measurements are preferred not only for single-pass diagnostics at different locations in a transfer line, but also to enable time resolved observations of a stored beam within a synchrotron. The essential reason for non-destructive diagnostics is the large beam power available at modern hadron accelerators, which excludes the usage of traditional intercepting methods like scintillation screens, SEM-grids or wire scanners due to the high risk of material damage during irradiation by the total beam intensity.

As an alternative to these traditional devices a Beam Induced Fluorescence (BIF) Monitor was realized and its properties were investigated in detail during the last years. A BIF Monitor is schematically depicted in Fig. 1. Due to the electronic stopping power the residual gas is ionized and left in an excited state with a certain probability. Optical photons emitted due to de-excitation can be used for transverse profile determination. But only those photons emitted towards the camera are detected, resulting in a solid angle $\Omega \simeq 10^{-4}$ and single photon technologies have to be applied. The spatial resolution is adapted to the beam parameters over a wide range by choosing an appropriate optical magnification ratio. An important boundary condition is the depth of field, which has to cover the entire beam diameter. The BIF method was investigated by different authors for profile measurements at cw-LINACs [1, 2, 3], pulsed LINACs [4, 5], cyclotron facilities and has been tested at synchrotrons as well [6, 7, 8].

* p.forck@gsi.de

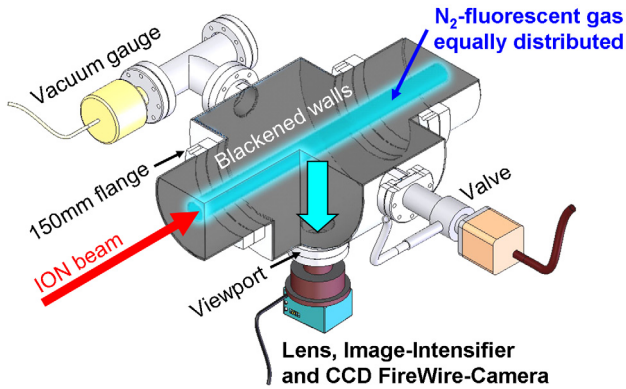

Figure 1: Scheme of a BIF Monitor for horizontal beam profile determination as installed at GSI.

TECHNICAL REALIZATION

In order to detect single photons an image intensified camera has to be used. One technical principle is the MCP-based image intensifier. In these devices the photon are converted to an electron at a photo-cathode and accelerated to a Multi-Channel-Plate (MCP). This might be either a single MCP having an $\sim 10^3$-fold amplification of photo-electrons or a double MCP stack with $\sim 10^6$-fold amplification, the latter one is suited for single photon detection. The electron avalanche hits a phosphor screen to create photons again which are finally observed by a standard CCD camera. The installations at GSI Ion LINAC comprises of either a tri-alkali photo-cathode S20 or bi-alkali photo-cathode in front of a double MCP stack of 25 mm diameter [9]. A standard lens system (in most cases Pentax C1614ER with focal length $f = 16$ mm) provides a reproduction scale of typically 250 µm per pixel [4]. For some of the experiments other lens system are used, e.g. with enhanced UV transmission (LINOS inspec.x with $f = 50$ mm). The spatial resolution is about 100µm (with respect to the beam location), mainly determined by the internal resolution of the double MCP intensifier arrangement. The resolution on the photo-cathode acting as the image plane is about 30 line-pairs per mm (lp/mm). CCD cameras with a digital interface (FireWire of GigE) are used to provide a loss-less data transport and adequate trigger possibilities [10].

As an alternative to MCP-based image intensifiers segmented photo-multipliers are used by other authors [6, 11]. As a third possibility a modern electron-multiplying CCD camera (emCCD) was considered [12, 13]: The amplification of the photo-electrons is realized by a chain of avalanche diodes between the CCD matrix and the ADC.

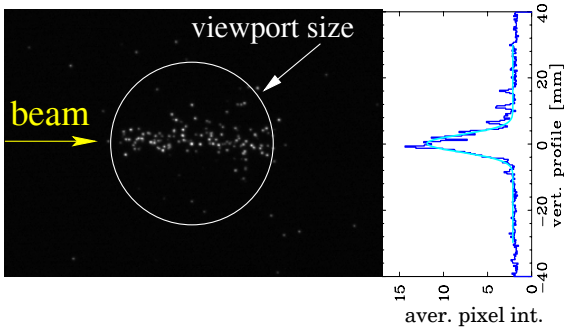

Figure 2: Two dimensional fluorescence image (left) of a Ar^{10+} beam at 4.7 MeV/u and I_{beam} = 2.5 mA recorded during one 250 µs long macro-pulse in 10^{-5} mbar N_2 and the projection for the vertical beam profile (right) [4].

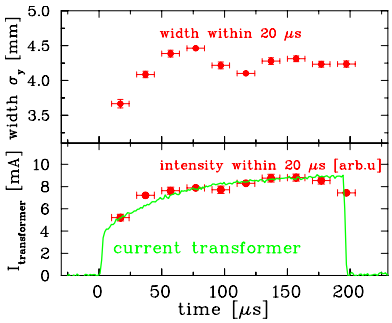

Figure 3: The beam width variation during a macro-pulse of 8 mA Ar^{10+} at 11 MeV/u is shown on top, the exposure time is 20µs . The lower graph compares the fluorescence yield (in arbitrary units) with the beam current [4].

RESULTS OBTAINED AT THE GSI-LINAC

At the pulsed GSI Ion LINAC BIF Monitors are installed at several locations and used for standard operation of high current beams [10]. An example is depicted in Fig.2 using a double MCP image intensifier capable of single photon detection. Each spot on the raw image corresponds to one photon. The projection shows sufficient statistical accuracy, which can be improved by smoothing algorithms due to the large reproduction scale of 300 µm per pixel. Beam profiles can be determined within one single macro-pulse of typically 100 µs length as used for the injection into the proceeding synchrotron SIS. The correspondence to SEM-Grid based measurements is good, e.g. the evaluated width, as characterized by the standard deviation, coincides better than 10 %.

An advanced application is the determination of a possible and in most cases unwanted variation of the beam profile during the macro-pulse, as shown in Fig. 3. Within a rise time of τ_{rise} = 100 ns the voltage between the photocathode and the MCP can be switched from blocking mode to photo-electron transmission toward the MCP. This can be used to restrict the exposure time during the profile measurement. In the case of Fig. 3 one image of 20 µs exposure time is recorded and these short term measurements are repeated with 10 different trigger delays. This type of time-resolved profile determination is not possible with an intersecting SEM-grid for the full macro-pulse length.

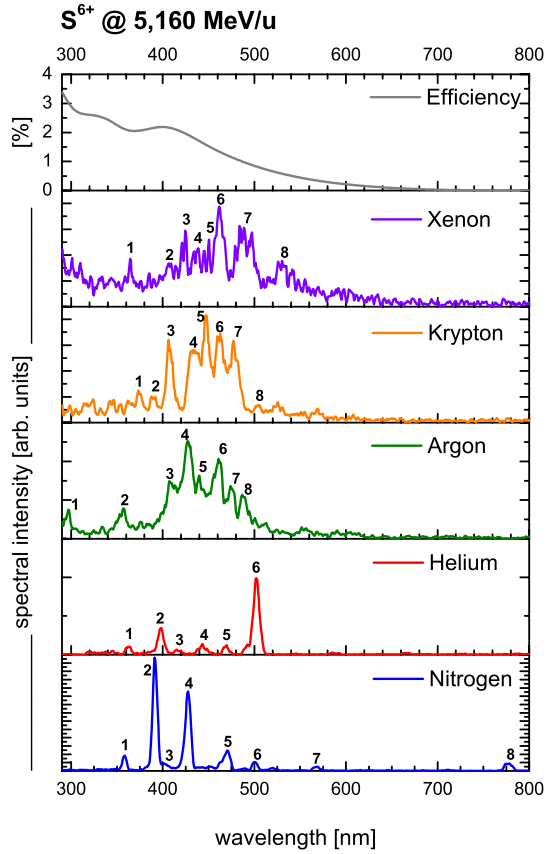

Figure 4: Optical beam induced spectra recorded with a beam of S^{6+} ions at 5.2 MeV/u in various gases of 10^{-3} mbar N_2-equivalent pressure [14]. The total efficiency of the optics and the image intensifier are are shown in the upper plot, the wavelength dependency is mainly determined by the S20 tri-alkali photo-cathode.

SPECTROSCOPIC INVESTIGATIONS

The driving mechanism for BIF is an effective conversion of the ion's energy loss to fluorescence photons in the optical wavelength range via an excited state of the residual gas. The fluorescence yield and the wavelength spectra of rare gases and N_2 are extensively investigated using an imaging spectrograph [14]. An example for a beam of medium heavy S^{6+} ions 5.2 MeV/u is depicted in Fig. 4. Separated lines are detected for N_2 as working gas within the relatively compact wavelength interval 392 nm $< \lambda <$ 460 nm. The prominent lines (number 1 to 5 in the displayed spectrum) correspond to a transition band to the N_2^+ electronic ground state (N_2^+: $B^2\Sigma_u^+(v') \rightarrow X^2\Sigma_g^+(v'') + \gamma$, for vibrational levels v). The lifetime of N_2^+ excited states were obtained by other authors to be τ = 58.0(3) ns, which coincides for 25 GeV [6, 7] and 100 keV [16] proton impact. For the case of *He* separated lines in the blue wavelength range are detected, originated by transition within

Table 1: Florescence yield Y of rare gases relative to N_2 and the yield normalized to the target electron density $Y_{dE/dx} = Y/Z$ for S^{6+} ions at 5.2 MeV/u using the data of Fig. 4 [14].

Gas	*Xe*	*Kr*	*Ar*	*He*	N_2
Y [%]	86	63	38	4	100
$Y_{dE/dx}$ [%]	22	25	30	26	100

the neutral *He* atom. For heavy rare gases broader spectra with overlapping lines were observed which are caused by transitions of the ionized atoms. Most lines were identified and are compiled in [15]. Comparable spectra were recorded for protons, Argon, Calcium, Tantalum and Uranium ions in the energy range from 4.33 MeV/u to 11.4 MeV/u [14, 15].

The wavelength integrated fluorescence yields Y of different working gases for impact of 5.2 MeV/u S^{6+} normalized to N_2 are compared in Table 1. For all gases an N_2-equivalent pressure of 10^{-3} mbar was used as determined by an Penning vacuum gauge. To overcome gas specific variations a cross calibration to a temperature corrected capacitance gauge was performed for each working gas, leading to an error of the actual pressure below 6 %. The related working gas density is sufficiently low to prevent second order excitations of the gas molecules via electron excitation like $N_2 + e^- \rightarrow N_2^* + e^- \rightarrow N_2 + \gamma + e^-$ [16], as the mean free path of electrons is much larger than the beam size of typically 10 mm. To include the energy loss dE/dx of the beam ions in the gas, the fluorescence yield $Y_{dE/dx}$ is normalized to the electron density represented by the atomic number of the working gas Z or $2Z$ for N_2. It has to be emphasized that the fluorescence yield per unit of energy loss of all rare gases is nearly similar but a factor of $\simeq 4$ lower compared to N_2 [14]. The absolute fluorescence yield was estimated for N_2 to be one optical photon per 3 keV of energy loss. Comparable results for N_2 and *Xe* working gas were obtained for proton impact in the energy range from 1.4 to 25 GeV at CERN [6].

Using an imaging spectrograph the beam profile of each individual spectral line can be obtained. For N_2 as the working gas all lines result in the same profile reading as displayed in Fig. 5 (middle). Slight variations are caused by the up-scaling of the noise due to normalization to the same maximum value. With exception of *He* the profile reading for all other investigated gases is independent of the selected spectral lines (for different wavelength intervals in the case of heavy rare gases). In Fig. 5 (top) the wavelength integrated profile readings are compared proving the stability of the profile determination independent of the working gas. However, in the case of *He* each spectral line (originated by the neutral atom) shows a significant but individual broadening of the beam image, see Fig. 5 (bottom). This behavior is independent of the ion beam species as confirmed for several ions from proton to Uranium at energies of around 5 MeV/u. Because the location of the photon emission does not represent the transverse profile

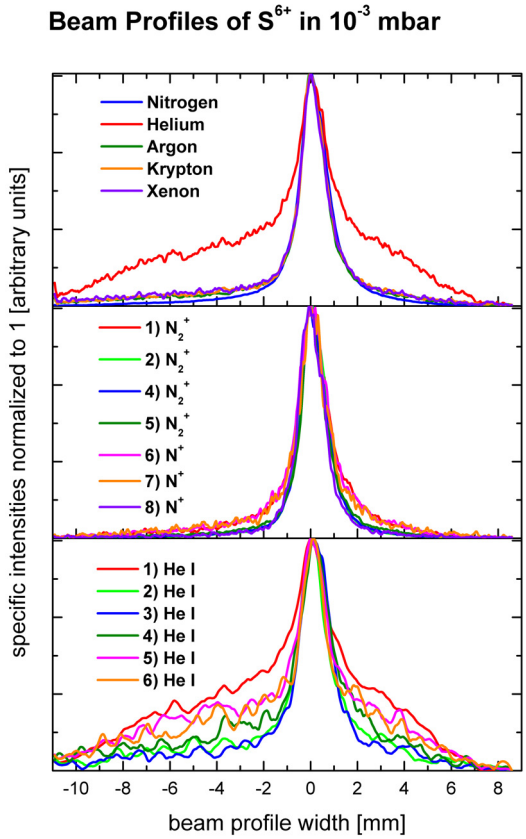

Figure 5: Gas specific beam profiles (upper plot) and transition specific beam profiles of nitrogen (middle) and helium (bottom), numbers as indicated in Fig. 4 [14].

He is excluded as a working gas.

Due to the high fluorescence yield and the spectral concentration in the blue wavelength range, N_2 offers the best performance and is well suited from a vacuum engineering point-of-view. Furthermore, the fluorescence yield of N_2 in the range 10^{-6} to 10^{-1} mbar is proportional to the pressure and the recorded profile width is independent of the pressure [5]. The only drawback is related to the relatively long lifetime $\tau = 58$ ns of the excited state of the ionic molecule N_2^+. For high intensity hadron beams with sub-mm width the N_2^+ ions might be displaced significantly by the beam's space charge prior to the photon emission. The effective image broadening depends strongly on the transverse beam density and pulse duration but is not significant for the achievable beam parameters at the present GSI facility. For the planned FAIR facility however, higher beam currents in connection with stronger focusing, in particular at the $\overline{\text{p}}$ and RIB production targets will lead to an intolerable image deformation. Using *Xe* as the working gas this image deformation can be significantly reduced. The lifetime of most Xe^+ transitions is only $\tau = 6.0(1)$ ns [6] and in connection with its large mass the acceleration within the beam's space charge is significantly smaller.

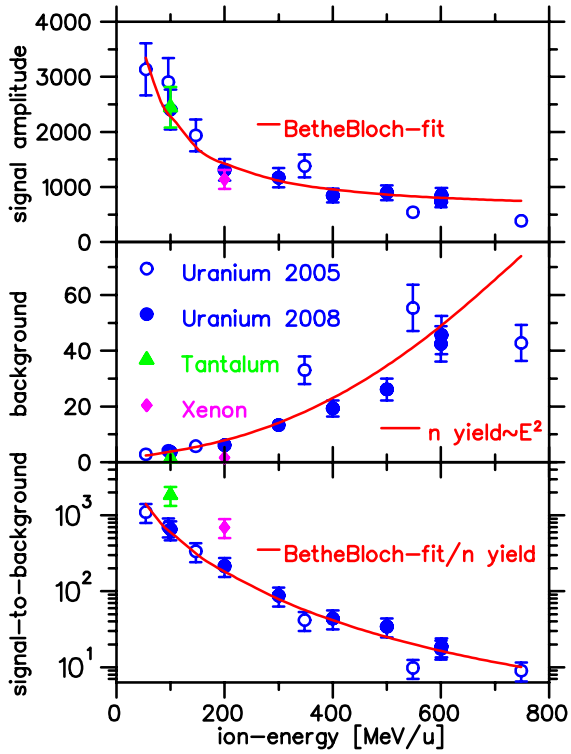

Figure 6: The signal amplitude (top), background level (middle) and signal-to-background ratio (bottom) as a function of energy for the investigated ions extracted from the GSI SIS18 synchrotron. The signal amplitudes for *Xe* and *Ta* were normalized by their charge and mass with respect to *U*. The background was normalized with respect to the mass only [5, 12].

SIGNAL AND BACKGROUND SCALING

For ion beams with energies up to GeV/u the BIF method was successfully tested at GSI with beams delivered from the GSI Heavy Ion Synchrotron SIS18. To investigate a possible installation close to a RIB or $\overline{\mathrm{p}}$ production target, the monitor was installed at the end of the transport line about 2 m upstream of a massive iron beam dump. For different ion beams, the integrated fluorescence yield in N_2 working gas for the energy range 60 MeV/u $< E_{kin} <$ 750 MeV/u is depicted in Fig. 6 (top). Since the energy loss in matter is described by the Bethe-Bloch formula, the signal strength of the investigated ions were fitted to this functional dependence, as additionally shown in Fig. 6 (top). The agreement to measured signal is quite good, proving the proportionality between energy loss and fluorescence yield for ions on a large energy scale. Comparable measurements were performed with protons in the energy range 50 MeV $< E_{kin} <$ 450 GeV at CERN [6, 7] for N_2 and *Xe* as working gas.

The most critical issue of the BIF method is the background contribution caused by neutron and γ radiation inducing photo-electron emission from the photo-cathode of the image intensifier. The background is uniformly distributed on the image and increases as a function of energy, as presented in Fig. 6 (middle). The independence on the iris opening and vacuum pressure judges that the background is not caused by optical photons. The main background contribution is generated at the photo-cathode but neither at the MCP nor the CCD chip. Charged particles can be excluded, due to their limited range in the surrounding material of the image intensifier. The background is therefore comprised of neutron and γ's with energies above several 100 keV. The neutron production Y_n per incident ion for energies $E_{kin} > 10$ MeV/u scales approximately with $Y_n \propto E_{kin}^2$, see e.g. [18]. Simulations of neutron and γ spectra for an 200 Mev/u *Xe* ions with PHITS and FLUKA were performed to evaluate the shielding concept for a monitor installation close to a beam dump, for more details see [12].

BACKGROUND SUPPRESSION

In order to use a BIF Monitor close to a target for high energetic beams an effective neutron and γ shielding is required. For typical beam parameters of energies around 1 GeV/u, as extracted from the GSI synchrotron SIS18, FLUKA simulations were performed [20]. The geometry was modeled according to the experimental conditions with the BIF monitor 2 m apart from the beam dump. The radiation level of the unshielded case was compared to the placement of the BIF-Monitor in the center of a $1 \times 1 \times 1$ m^3 concrete block. For an Ar^{18+} beam at 900 MeV/u the simulation predicts a reduction of the γ flux by 96 % and the neutron flux by 94 %, respectively.

For the arrangement of a shielded BIF Monitor, the fluorescence photons have to be transported to the sensor either by a telescope arrangement or by a fiber image bundle [12]. A flexible 1.2 m long fiber image bundle from company Schott [21] was used. It consists of about 10^6 fibers with Ø10 µm. It is mounted between the lens system and the image intensifier. The resolution of the fiber image bundle is about 45 lp/mm, which is superior to the image intensifier resolution of 35 lp/mm. The functionality of this arrangement was successfully tested with a low energetic beam of 11.4 MeV/u Ni^{13+}: The measured images and related profiles do not show any significant difference in terms of image quality and resolution.

Any type of γ, neutron or charged particle radiation passing the image bundle might causes scintillation light, which cannot be easily distinguished from the residual gas fluorescence. To estimate this effect, a BIF arrangement with and without an unshielded image bundle was installed at the same location and tested with an Ar^{18+} beam with 300 MeV/u: The increase of background due to scintillation of the image bundle arrangement was only about 30 %. From this finding we expect that for an image bundle enclosed in a concrete shielding the additional background from scintillation can be neglected. This will be experimentally investigated in near future. Other fiber bundle arrangements are proposed or tested in [3, 17].

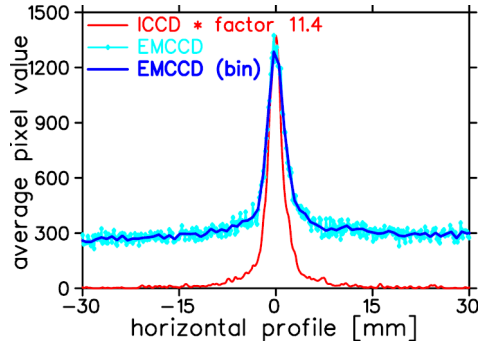

Figure 7: Beam profiles for a 60 µA Ni^{13+} beam with 11.4 MeV/u and 1.2 ms pulse duration in 10^{-4} mbar N_2 recorded with image intensifier CCD (8-bit) and emCCD (16-bit) camera. To compensate the higher spatial resolution of the emCCD, profile was binned by a factor 5.

ELECTRON MULTIPLYING CCD

A competing technique for single-photon detection is the Electron Multiplying CCD (emCCD). Its CCD chip has up to ≃ 10-fold higher quantum efficiency (depending on the chip properties) compared to the photo-cathode of an image intensifier. This camera type is equipped with an additional amplification stage, based on avalanche diodes between the CCD shift register and output amplifier. The tested Hamamatsu C-910013 camera has a back illuminated sensor and is Peltier-cooled down to -80^{o}C. This system was compared to the image intensifier as depicted in Fig. 7. In general, the emCCD has a higher noise contribution due to the thermal noise of the electronics amplification chain. This background is avoided by a MCP-based system due to the amplification by secondary electrons. Especially under single photon counting conditions at GSI, this is a important issue. However, the emCCD camera has a ≃ 5-fold higher spatial resolution, because of constantly small single photon spots, even at the highest gain level. In contrary, the MCP-based system shows increasing spots sizes for increasing gain levels. The higher quantum efficiency of an emCCD is an advantage but has to be weighted with the noise contribution.

CONCLUSION

The BIF method for beams from 1.4 to 750 MeV/u was carefully investigated during the last years and a standard realization is now available for accelerator operation at GSI. Due to the single photon detection efficiency and the possibility of gating, MCP-based image intensifiers are well suited for measurements with an exposure time down to 100 ns to match the exposure time to the beam delivery or to visualize possible fast beam variations. Modern emCCD cameras might be an alternative with a higher spatial resolution. The signal strength is proportional to the stopping power. By changing the working gas pressure up to 1 mbar the photon rate can be adjusted without significant image distortions. Different working gases were investigated with the result that N_2 provides the highest light yield in a compact wavelength interval. Moreover, it is well suited from a vacuum technology point-of-view. The only disadvantage is the relatively long lifetime of the excited states. For intense beams, a distorted profile reading due to the N_2^+ movement prior to the light emission is possible and have to be estimated with appropriate particle tracking calculations. Using *Xe* as a working gas this contribution can be reduced significantly due to ≃10-fold shorter lifetime and ≃5-fold higher mass. For all observed cases *He* is excluded as a working gas.

The image sensor is sensitive to neutron and γ radiation. For higher beam energies and close to a beam dump, a shielding is mandatory. Photon guidance in a fiber image bundle was successfully demonstrated. This allows installations of BIF-Monitors even in the vicinity of a production target.

For the profile measurement of beams circulating in a synchrotron, the applicability of the BIF method has to be checked carefully: Due to the lower vacuum pressure the photon rate might be too low for the anticipated time resolution. For this application Ionization Profile Monitors (IPM) [22] might be better suited due to their '4π detection scheme' of residual gas ions or electrons. But IPMs require a lot more mechanical and electronic efforts compared to a BIF installation.

REFERENCES

[1] D.P. Sandoval et al., *BIW'93*, p. 273 (1993).
[2] D.D. Chamberlin et al., Proc. PAC'81, p. 2347 (1981).
[3] J.M. Carmona et al., *DIPAC'09*, p.173 (2009) and J.M. Carmona, these proceedings.
[4] P. Forck, A. Bank, *EPAC'02*, p. 1885 (2002) and A. Bank, P. Forck, *DIPAC'03*, p. 137 (2003).
[5] F. Becker et al., *DIPAC'07*, p. 33 (2007).
[6] M.A. Plum et al., *Nucl. Instrum. Meth* **A 492**, p. 42 (2002).
[7] A. Variola, R. Jung, G. Ferioli, *Phys. Rev. Acc. Beams* **10**, 122801 (2007), G. Burtin et al., *EPAC'00*, p. 256 (2000).
[8] T. Tsang et al., *PAC'09*, p. 1 (2009) and T. Tsang et al., *Rev. of Sci. Instrum.* **79**, 105103 (2008).
[9] E.g. company Proxitronic, www.proxitronic.com.
[10] R. Haseitl et al., *DIPAC'09*, p. 134 (2009) and C. Andre et al., *GSI Scientific Report 2008*, p. 124 (2009).
[11] C. Böhme et al., *BIW'10* (2010).
[12] F. Becker et al., *BIW'08*, p. 236 (2008).
[13] See e.g. www.emccd.com.
[14] F. Becker et al., *DIPAC'09*, p. 161 (2009) and F. Becker et al., *BIW'10* (2010).
[15] F. Becker, *Non-destructive Profile Measurement of intense ion beams,* PhD-Thesis, Darmstadt 2009.
[16] R.H. Hughes et al., *Phys. Rev.* **123**, 2084 (1961), L.W. Dotchin et al., *J. Chem. Phys.* **59**, 3960 (1973).
[17] F. Senee et al., *DIPAC'09*, p. 197 (2009).
[18] T. Kurosawa et al., *Phys. Rev. C*, **62**, 044615 (2000).
[19] H. Iwase, privat communication (2008).
[20] A. Plotnikov, private communication (2009).
[21] Company Schott, www.us.schott.com
[22] See e.g. P. Forck, *IPAC'10*, p. 1261 (2010).